# Finite-Element Analysis of a Shielded Pulsed-Current Induction Heater – Experimental Validation of a Time-Domain Thin-Shell Approach

Ruth V. Sabariego[1], Peter Sergeant[2,3], Johan Gyselinck[4], Patrick Dular[1,5], Luc Dupré[2] and Christophe Geuzaine[1]

[1]Dept. of Electrical Engineering and Computer Science (ACE), University of Liége, Belgium, E-mail: R.Sabariego@ulg.ac.be
[2]Dept. of Electrical Energy, Systems and Automation, Ghent University, Belgium
[3]Dept. Electrotechnology, Faculty of Applied Engineering Sciences, University College Ghent, B-9000 Ghent, Belgium
[4]Dept. of Bio-, Electro- and Mechanical Systems (BEAMS), Université Libre de Bruxelles (ULB), Belgium
[5]Fonds de la Recherche Scientifique, F.R.S.-FNRS, Belgium

***Abstract* — A time-domain extension of the classical frequency-domain thin-shell approach is used for the finite-element analysis of a shielded pulse-current induction heater. The time-domain interface conditions at the shell surface are expressed in terms of the average instantaneous flux density vector in the shell, as well as in terms of a limited number of higher-order components. The three-dimensional thin-shell model is validated by comparing the numerical results with measurements performed on the heating device at different working frequencies.**

## I. INTRODUCTION

Conducting pieces can be thermally treated by means of induction heaters that generate strong alternating magnetic fields and induce eddy currents in them. Traditionally the current source of these heating devices was sinusoidal. However, the use of pulsed currents becomes a very attractive alternative thanks to several interesting technological effects. Specifically, it allows to reduce the inductor dimensions and to achieve a more uniform warming [1].

The shielding of these devices is often crucial to mitigate the magnetic field in its environment and reduce the hazardous exposure of both the human operator and the electronic equipment. In practice, these shields are thin metallic sheets with holes to guarantee the accessibility to the heater (to guide control or power wires, to allow cooling...). Their numerical modelling becomes thus an essentially 3D task.

The finite element (FE) analysis of these magnetic shielding problems involving thin shells may suffer from both meshing difficulties and high computational cost. The well-known thin-shell approach allows to overcome these troubles, but it is most often restricted to linear and time-harmonic analyses [2, 3, 4].

Considering a pulsed current as heating source demands a time-domain model. In [5] a pure time-domain approach with the magnetic vector potential formulation is proposed. It is based on the use of orthogonal polynomial basis functions to account for the variation of the magnetic flux through the shell thickness. The method is further extended to the magnetic field formulation in [6].

This paper deals with the analysis of a shielded induction heater with a pulsed current. Numerical results obtained with a time-domain thin-shell approach are compared with measurements performed on an experimental setup.

## II. MAGNETODYNAMIC FORMULATION

We consider a magnetodynamic problem in a bounded domain $\Omega = \Omega_c \cup \Omega_c^C \in \mathbb{R}^3$ with boundary $\Gamma$. The conductive and non-conductive parts of $\Omega$ are denoted by $\Omega_c$ and $\Omega_c^C$. Source inductors constitute domain $\Omega_i \subset \Omega_c^C$ (Fig. 1).

The Maxwell equations and constitutive laws governing the low-frequency eddy-current problems are

$$\operatorname{curl} h = j\,,\ \operatorname{div} b = 0\,,\ \operatorname{curl} e = -\partial_t\, b\,,\ b = \mu h\,,\ j = \sigma e\,, \tag{1 a-e}$$

where $h$ is the magnetic field, $b$ the magnetic flux density (or induction), $e$ the electric field, $j$ the electric current density, $\mu$ the permeability (reluctivity $\nu = 1/\mu$) and $\sigma$ the conductivity (resistivity $\rho = 1/\sigma$).

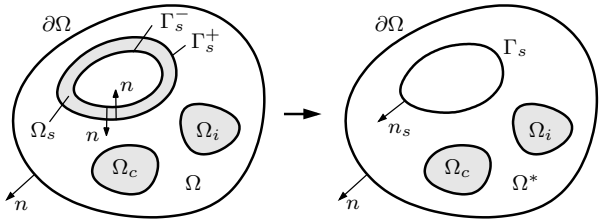


Fig. 1. Bounded domain $\Omega$ and reduction of the thin-shell volume $\Omega_s$ to the surface $\Gamma_s$

The $a-$formulation is obtained from the weak form of the Ampère law (1 a):

$$(\nu \operatorname{curl} a, \operatorname{curl} a')_\Omega + (\sigma\, \partial_t a, a')_{\Omega_c} + \langle n \times h, a' \rangle_\Gamma = (j_i, a')_{\Omega_i}\,, \tag{2}$$

where $a$ is the magnetic vector potential; $n$ is the outward unit normal vector on $\Gamma$; $j_i$ is a prescribed current density; $(\cdot,\cdot)_\Omega$ and $\langle \cdot,\cdot \rangle_\Gamma$ denote a volume integral in $\Omega$ and a surface integral on $\Gamma$ of the scalar product of their arguments.

The first step in the thin-shell approach consists in reducing the thin-shell volume $\Omega_s \subset \Omega_c$ (thickness $d$) to an average surface $\Gamma_s$ situated halfway between the inner surface $\Gamma_s^-$ and outer surface $\Gamma_s^+$ of $\Omega_s$ (outward normal $n_s$), as depicted in Fig. 1. Next the surface integral in (2) is modified on the basis of the 1-D thin-shell model described hereafter.

## III. 1-D THIN-SHELL MODEL

In the 1-D model of the shell, only the variation of the magnetic field $h(z,t)$ and the magnetic induction $b(z,t)$ tangential to the boundary of the shell $\Gamma_s$ is considered throughout the shell thickness. We adopt a local coordinate system $xyz$ with the $z-$axis normal to the shell (i.e. parallel to $n_s$) and $z = 0$ at its center. The tangential components of the magnetic field $h$ on $\Gamma_s^+$ and $\Gamma_s^-$ (both sides of the shell) are defined as:

$$h_t^+ = n_s \times (h|_{\Gamma_s}^+ \times n_s)\,, \quad h_t^- = n_s \times (h|_{\Gamma_s}^- \times n_s)\,. \tag{3 a b}$$

This work is partly supported by the Belgian Science Policy (IAP P6/21).

Analogously to (3), hereafter $f_t$ denotes the tangential component of a field $f$ on a surface $\Gamma$ with normal $n$.

### A. Governing differential equation

The 1-D eddy-current problem in the shell ($-d/2 \le z \le d/2$) is governed by:

$$\partial_z^2 h_t(z,t) = \sigma\, \partial_t b_t(z,t)\,, \tag{4}$$

with constitutive law $h_t(z,t) = \nu\, b_t(z,t)$. The associated boundary conditions on the upper (+) and lower (−) surfaces of the shell are given by $h_t^{\pm}(t) = h_t(\pm d/2, t)$.

### B. Harmonic case

For a sinusoidal time variation at pulsation $\omega$, we define the relative shell thickness as $d/\delta$, with $\delta = 1/\sqrt{2/\sigma\mu\omega}$ the penetration depth.

Under these assumptions (4) can be solved analytically, which leads to an expression in terms of the complex representation (symbols in bold) of $h_t^+(t)$, $h_t^-(t)$ and $b_0(t)$ [2]:

$$\boldsymbol{h}_t^+ + \boldsymbol{h}_t^- = 2\,\nu\, \boldsymbol{Y}(d/\delta)\, \boldsymbol{b}_0\,, \tag{5}$$

with $\boldsymbol{Y}(d/\delta) = \frac{1+\boldsymbol{\imath}}{2}\, d/\delta \operatorname{cotanh}\left(\frac{1+\boldsymbol{\imath}}{2}\, d/\delta\right)$, where $\boldsymbol{\imath}$ is the imaginary unit.

The well-known FE frequency-domain approach includes the 1-D thin-shell model in a 2-D and 3-D analysis via the tangential fields $h_t^+$, $h_t^-$ and (5) as done in [2, 3, 4].

### C. Time-domain extension

We now develop a time-domain extension of (5) by considering $n+1$ polynomial basis functions for the expansion of the tangential induction $b_t(z,t)$ [5, 6]. We choose a set of orthogonal Legendre polynomials $\alpha_k(z)$ to expand $b_t(z,t)$, i.e. ,

$$b_t(z,t) = \sum\nolimits_{k=0}^{n} \alpha_k(z)\, b_k(t)\,, \tag{6}$$

with $|\alpha_k(\pm d/2)| = 1$.

Strongly satisfying (4), the magnetic field $h_t(z,t)$ can be written as

$$h_t(z,t) = \frac{h_t^+(t) + h_t^-(t)}{2} + \frac{h_t^+(t) - h_t^-(t)}{d}\, z + \sigma d^2 \sum\nolimits_{k=0}^{n} \beta_k(z)\, \partial_t b_k(t)\,, \tag{7}$$

where $d^2\, \partial_z^2\, \beta_k = \alpha_k(z)$ and $\beta_k(\pm d/2) = 0$.

Next, with a finite number of basis functions, the constitutive law $h(z,t) = \nu\, b(z,t)$ can be weakly imposed as:

$$\int_{-d/2}^{d/2} \alpha_k(z) \Big( h_t(z,t) - \nu\, b_t(z,t) \Big)\, \mathrm{d}z = 0\,, \tag{8}$$

which leads to $n+1$ differential equations ($k = 0, \ldots, n$) in terms of $b_0(t), \ldots, b_n(t)$, $h_t^+(t)$ and $h_t^-(t)$ [5, 6].

The following system of linear differential equations is obtained:

$$[H(t)] = \nu\, [P]\, [B(t)] + \sigma d^2\, [Q]\, \partial_t [B(t)]\,, \tag{9}$$

with $[H(t)] = \left[\frac{h_t^+ + h_t^-}{2}\ \frac{h_t^+ - h_t^-}{6}\ 0\ \cdots\ 0\right]^T$ and $[B(t)] = [b_0(t)\ b_1(t)\ \cdots\ b_n(t)]^T$. The elements $p_k$ and $q_{kl}$ ($k, l = 0, \ldots, n$) of the diagonal matrix $[P]$ and triangular matrix $[Q]$ are given by:

$$p_k = \int_{-d/2}^{d/2} \alpha_k(z)\, \alpha_k(z)\, \mathrm{d}z\,, \quad q_{k,l} = \int_{-d/2}^{d/2} \alpha_k(z)\, \beta_l(z)\, \mathrm{d}z\,. \tag{10}$$

## IV. FE IMPLEMENTATION

In the thin-shell formulation, the thin-shell volume $\Omega_s$ is excluded from the original calculation domain $\Omega$. Further, the surface $\Gamma_s$ with outward normal $n_s$ and situated halfway between the inner surface $\Gamma_s^-$ and outer surface $\Gamma_s^+$ of $\Omega_s$ is added to the new domain $\Omega \backslash \Omega_s$ (Fig. 1). In order to account for the changes in these domains, the surface integral term in (2) is modified [5, 6]. The new weak form reads:

$$(\nu \mathrm{curl}\, a, \mathrm{curl}\, a')_{\Omega\backslash\Omega_s} + (\sigma\, \partial_t a, a')_{\Omega_c} + \langle n \times h, a' \rangle_{\Gamma} + \langle n_s \times h, a' \rangle_{\Gamma_s^-} - \langle n_s \times h, a' \rangle_{\Gamma_s^+} = (j_i, a')_{\Omega_i}\,. \tag{11}$$

The time-domain behavior of the thin shell is taken into account by introducing the tangential vector fields $b_0$, $b_1$, $\cdots$ $b_n$ on $\Gamma_s$ as unknowns.

Taking into account the boundary conditions $h_t^{\pm}(t) = h_t(\pm d/2, t)$ in the 1-D eddy current problem and the Ampère law (1 a), the tangential component of the magnetic field $h_t$ is discontinuous across $\Gamma_s$ and related to the net current $d\, j_0$ in the shell as

$$h_t^+ - h_t^- = -n_s \times d\, j_0(t)\,, \tag{12}$$

with $j_0(t)$ the average current density vector tangential to $\Gamma_s$. Moreover, the tangential component of the magnetic vector potential $a_t$ is also discontinuous across $\Gamma_s$ and is related to the net flux $d\, b_0$ in the shell as

$$a_t^+ - a_t^- = -n_s \times d\, b_0(t)\,, \tag{13}$$

with $b_0(t)$ the average flux density vector tangential to $\Gamma_s$.

We therefore decompose $a$ as $a_c + a_d$, the tangential components of $a_c$ and $a_d$ being continuous and discontinuous across the shell, respectively.

Without loss of generality we can choose $a_d$ to be zero in the volume enclosed by $\Gamma_s$. Furthermore, conformity can be ensured by limiting its support to one layer of elements touching $\Gamma_s^+$ [4]. By considering $a^- = a_c$ and $a_d = -n_s \times d\, b_0$ together with (12), we can work out the two new surface terms in (2). They are given by

$$\begin{aligned} &\langle n_s \times h, a' \rangle_{\Gamma_s^-} - \langle n_s \times h, a' \rangle_{\Gamma_s^+} \\ &= -\langle n_s \times h_t^+, a_c' \rangle_{\Gamma_s} - \langle n_s \times h_t^+, a_d' \rangle_{\Gamma_s} + \langle n_s \times h_t^-, a_c' \rangle_{\Gamma_s} \\ &= d \langle h_t^+, b_0' \rangle_{\Gamma_s} - d \langle j_0, a_c' \rangle_{\Gamma_s}\,. \end{aligned} \tag{14}$$

From the first two lines of system (9) we get an expression for $h_t^+$ and $h_t^-$ in terms of $b_0$, $b_1$, $b_2$ and $b_3$ (assuming $n \ge 2$):

$$\begin{aligned} h_t^{\pm} = {} & \nu\, b_0 + \sigma d^2 (q_{00} \partial_t b_0 + q_{02} \partial_t b_2) \\ & \pm 3\, \nu\, b_1 \pm 3\, \sigma d^2 (q_{01} \partial_t b_1 + q_{03} \partial_t b_3)\,. \end{aligned} \tag{15}$$

The weak form (11) is thus coupled with the time-domain thin-shell approximation via $a_c$, $a_d$ in $\Omega \backslash \Omega_s$ and $b_0$, $b_1$, $b_2$ and $b_3$ on $\Gamma_s$.

Next, from (12) and (7), we get the second condition concerning the tangential components $a_{c,t}$ and $a_{d,t}$ of $a_c$ and $a_d$. We have:

$$-\sigma \partial_t (2 a_{c,t} + a_{d,t})/2 = \frac{2}{d} \nu b_1 + \sigma d \Big( \frac{1}{5} \partial_t b_1 - \frac{1}{70} \partial_t b_3 \Big)\,, \tag{16}$$

which we can weakly imposed on $\Gamma_s$ with test functions $b_1'$ and $b_3'$.

The remaining equations of system (9) result in the following weak forms with test functions $b_l'$ ($l = 2, 3, \cdots, n$):

$$0 = \langle \nu\, p_l\, b_l, b_l' \rangle_{\Gamma_s} + \sum_{i=-2,0,2} \langle \sigma d^2\, q_{l,l+i}\, \partial_t b_{l+i}, b_l' \rangle_{\Gamma_s}\,. \tag{17}$$

## V. ANALYSIS OF THE INDUCTION HEATER

The induction heater comprises a pulsed-current excitation coil and a cylindrical shield (190 mm high), made either of copper (0.5 mm wide, $\sigma = 5.3\,10^7$ S/m) or steel (0.65 mm wide, $\sigma = 5.9\,10^6$ S/m, $\mu_r = 372$). The steel shield has circular perforations of 76 mm diameter; two holes aligned in the axial direction and repeated periodically along the circumference. The distance between the holes in the axial and azimuthal directions is approximately the same. The workpiece is a cylindrical aluminium plate (radius = 191 mm, height = 10 mm, $\sigma = 3.7\,10^7$ S/m,$\mu_r = 1$). The induction heating setup is shown in Fig. 2.

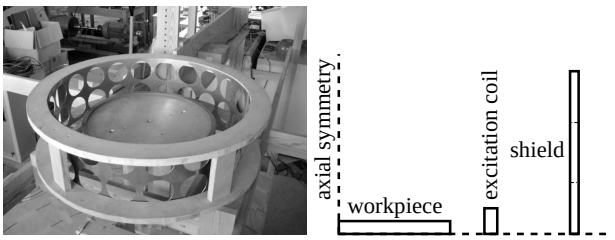


Fig. 2. Picture of the studied induction heating application (left). Sketch of the setup (right)

Although the current waveforms in a pulsed induction heater are usually generated by a power electronic converter, the waveforms used in our experimental setup (see Fig. 3) are imposed by a linear amplifier. The amplitude of the current is about 10 times smaller than in the induction heating device in [1], but the results can be rescaled because our setup does not contain nonlinear materials whose electromagnetic properties (such as permeability) change with the field amplitude.

The generation of the waveform signals for the linear amplifier was done by a National Instruments PCI-6110 card, controlled by LabVIEW. The pulsed current waveform, generated for a given frequency and peak current, is programmed based on the analytical expression found in [1] and consists of three parts: part 1 where a capacitor is charged (load current is zero), part 2 where the capacitor is discharged (load current increases and reaches maximum) and part three where the capacitor is short-circuited (load current decreases to zero). The output of the linear amplifier differs from the input waveform especially for the highest considered frequency, due to the limited slew rate of the amplifier (see Fig. 3). Note that the three curves in Fig. 3 are not in phase due to the lack of triggering when measuring. This phase displacement could be easily avoided though it would not influence the quality of the results.

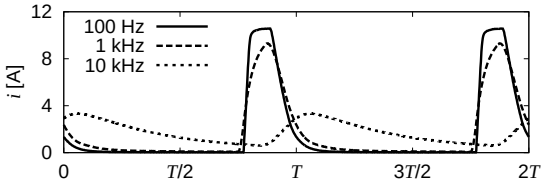


Fig. 3. Measured pulsed current at different frequencies: $f = 100$ Hz, 1 kHz and 10 kHz (period $T = 1/f$)

The current waveform and the magnetic induction waveform were measured by a Tektronix current probe and an inductive magnetic field sensor respectively. Both signals were sampled simultaneously at 500 samples per period, resulting in a maximal sample rate of 5 MS/s at 10 kHz. Measurements were carried out with the excitation coil working at three different frequencies 100 Hz, 1 kHz and 10 kHz and in the presence of the aluminum plate for the following situations: with no shield; with an axisymmetric copper shield and with a perforated shield in steel (see Fig. 2).

Time-stepping simulations with imposed measured pulsed current at three different frequencies $f = 100$ Hz, 1 kHz and 10 kHz are carried out. A period $T = 1/f$ is time-stepped with $\Delta t = T/120$. Two periods of the simulation results in steady-state are compared with the performed measurements. In all considered cases, the measured and computed vertical components of the magnetic flux density $b$ are compared at a point outside the shield in the symmetry plane (50 cm from the center of the device, 20 cm from the shield position). The time-domain thin-shell approach is applied to model the shield.

In order to have an idea of quality of the measurements, we consider first the case with no shield. An excellent agreement is observed in Fig. 4.

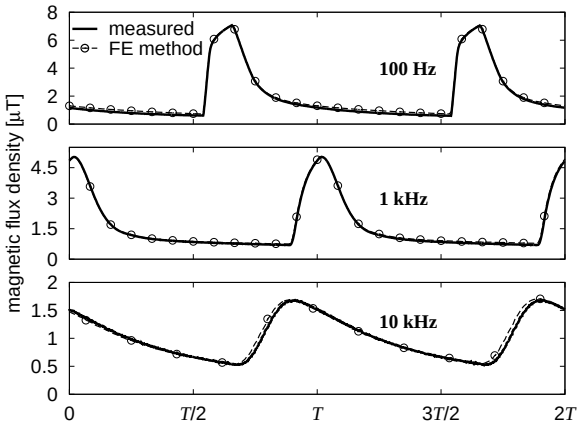


Fig. 4. Vertical component of magnetic flux density at a distance of 50 cm from the center of the induction heater, no shield considered

Then a cylindrical copper shield is added to the setup. The thin-shell approach is applied to the shield in an axisymmetric model. Results are depicted in Fig. 5. The measurements are quite noisy at 1 kHz and 10 kHz due to the small amplitude variation of the magnetic field outside the shield. At all considered frequencies, there is hardly any skin effect (uniform distribution of the eddy currents), so that the thin-shell method gives a good approximation with $n = 0$ (only two additional unknowns on $\Gamma_s$: $b_0$ and $b_1$). Indeed, the difference between results for $n = 0$ and $n = 2$ at 1 kHz and 10 kHz is negligible.

Eventually, the perforated steel shield depicted in Fig. 2 is studied. A full 3-D FE model is used (see detail of the 3-D mesh in Fig. 6). The nonlinearity of the steel is not taken into account in the simulations but is proved to be negligible by the results hereafter. At 100 Hz, there is hardly any skin effect, and thin-shell approximation is already excellent with $n = 0$. At 10 kHz, the skin effect is much more important. The thin-shell approach with $n = 2$ (additional unknowns on $\Gamma_s$: $b_0$, $b_1$, $b_2$ and $b_3$) gives a quite good approximation though. The numerical model shows thus a very good correlation with the measurements.

### A. Computational cost

In order to highlight the interest of the proposed thin-shell method, we analyze the computational data for the induction heater shielded with a perforated steel layer. The system of

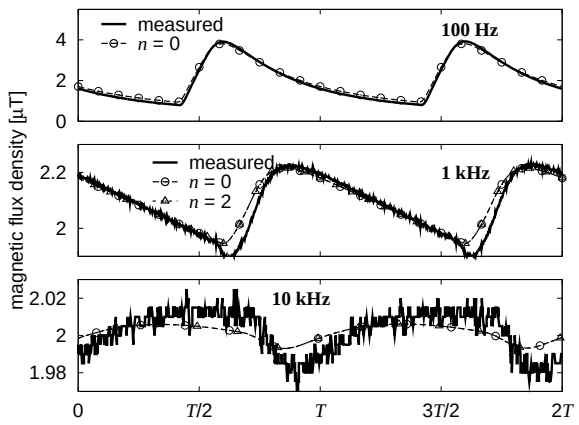


Fig. 5. Vertical component of magnetic flux density at a distance of 50 cm from the center of the induction heater and outside a cylindrical copper shield

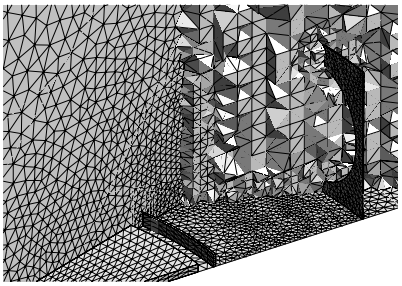

Fig. 6. Detail of the 3D mesh (right)

algebraic equations is solved by means of an LU direct solver on a MacBook Pro with a 2.4 GHz Intel Core 2 Duo Processor.

The 3-D FE models employ a support mesh (see Fig. 6) that yields $N$ complex unknowns. In the conventional FE method, this value $N$ increases with the number of layers along the shield thickness used for discretising it, what depends in turn on the working frequency (the higher the frequency, the higher the number of required layers). Besides the huge difference between the width of the shield and its other dimensions makes the meshing task considerably arduous. With the thin-shell approach, the shield is modeled by a surface and the mesh remains the same for all considered frequencies, which is the main advantage of the method. $N$ augments with a fix and reduced value of complex unknowns when increasing $n$ (e.g. 1279 new unknowns for a unitary increment and the mesh considered in Table I).

TABLE I. Computation time (per time-step) for the conventional FE method and the thin-shell approach

| 3-D FE model | | | Thin-shell approach | | |
|---|---|---|---|---|---|
| layers | $N$ | $t$ (s) | n | $N$ | $t$ (s) |
| 2 | 71384 | 35 | 0 | 65589 | 30 |
| 4 | 74266 | 42 | 2 | 68147 | 33 |
| 6 | 85098 | 54 | 4 | 70705 | 35 |
| 8 | 91466 | 63 | 6 | 73263 | 42 |
| 10 | 97747 | 66 | | | |

Let us analyse an example shown in Table I. At 10 kHz, a number of 4 layers was required for ensuring good results with the conventional 3-D FE method. When using the thin-shell approach the reduction in computational is 28 % for $n = 0$, 21 % for $n = 2$, 17 % for $n = 4$ and there is no gain for $n = 6$. For the problem at hand, the accuracy of the

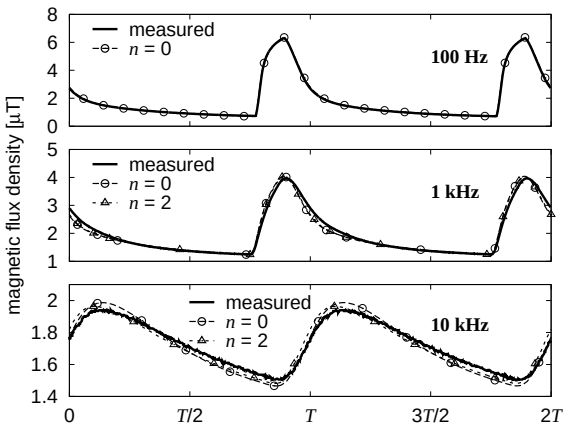


Fig. 7. Vertical component of magnetic flux density at a distance of 50 cm from the center of the induction heater and outside a perforated steel shield

approximation is high enough with $n = 2$. We would only need to increase $n$ for higher frequencies, and in that case the number of layers in the conventional model should also be increased. See Table I for further results.

## VI. CONCLUSIONS

A time-domain finite-element method for the analysis of thin-shells has been validated with measurements. The method is based on the coupling of a time-domain 1-D thin-shell model with a magnetic vector potential formulation via the surface integral term. A limited number of additional unknowns for the magnetic flux density are incorporated on the shell boundary.

An very good agreement between measurements and simulations is observed. A clear advantage of the proposed thin-shell approach is that the mesh of the computation domain does not depend on the working frequency anymore. It provides a good compromise between computational cost and accuracy. Indeed, adding a sufficiently high number of induction components in the thin-shell, a very high accuracy can be achieved.

## REFERENCES

[1] A. Shenkman, Y. Berkovich, and B. Axelrod, "Pulse converter for induction-heating applications," *IEE Proceedings – Electric Power Applications*, vol. 153, no. 6, pp. 864–872, 2006.

[2] L. Krähenbühl and D. Muller, "Thin layers in electrical engineering. example of shell models in analyzing eddy-currents by boundary and finite element methods," *IEEE Trans. on Magn.*, vol. 29, no. 5, pp. 1450–1455, 1993.

[3] I. D. Mayergoyz and G. Bedrosian, "On calculation of 3-D eddy currents in conducting and magnetic shells," *IEEE Trans. on Magn.*, vol. 31, no. 3, pp. 1319–1324, 1995.

[4] C. Geuzaine, P. Dular, and W. Legros, "Dual formulations for the modeling of thin electromagnetic shells using edge elements," *IEEE Trans. on Magn.*, vol. 36, no. 4, pp. 799–803, 2000.

[5] J. Gyselinck, R. V. Sabariego, P. Dular, and C. Geuzaine, "Time-domain finite-element modelling of thin electromagnetic shells," *IEEE Trans. on Magn.*, vol. 44, no. 6, pp. 742–745, June 2008.

[6] R. V. Sabariego, C. Geuzaine, P. Dular, and J. Gyselinck, "h- and a- time-domain formulations for the modelling of thin electromagnetic shells," *IET Science, Measurement & Technology*, vol. 2, no. 6, pp. 402–408, November 2008.